Knowledge-based Engineering and Sciences (2025), **6**, (3), 65–84
doi:10.51526/kbes.2025.6.3.65-84

RESEARCH PAPER

The Impact of Land Use and Land Cover on Land Surface Temperature and Urban Heat Islands using Geographical Information System and Remote Sensing: A Representative Case Study in Afghanistan

Najibullah Wali,[1,2] Abdul Habib Zaray,[3] Abdul Wahid Wahidi,[3] Ahmad Bilal Ahmadullah,[4] and Ziaul Haq Doost[*,5]

[1]Department of Architecture, Kandahar University, Kandahar 3801, Afghanistan
[2]Department of Architectural Engineering and Construction Management, King Fahd University of Petroleum and Minerals, Dhahran, Saudi Arabia
[3]Department of Civil Engineering, Engineering Faculty, Kandahar University, Kandahar 3801, Afghanistan
[4]Department of Energy Engineering, Engineering Faculty, Kandahar University, Kandahar 3801, Afghanistan
[5]Department of Civil and Environmental Engineering, King Fahd University of Petroleum and Minerals, Dhahran, Saudi Arabia
*Corresponding author. Email: ziaulhaq.doost@gmail.com

(Received 18 September 2025; revised 13 December 2025; accepted 26 December 2025; first published online 31 December 2025)

Abstract

This study investigated the transformation of land use and land cover (LULC) in Kandahar City, Afghanistan, and its subsequent impact on land surface temperature (LST) and the urban heat island (UHI) effect between 2008 and 2018. Employing geographic information system (GIS) and remote sensing (RS) techniques, the analysis revealed a 20.8% expansion in built-up areas and a corresponding 12.5% reduction in vegetation cover and agricultural lands. This shift resulted in a rise in mean LST from 30.1 °C in 2008 to 33.1 °C in 2018, with hotspot regions exceeding 41.75 °C. The results confirmed that urbanized zones with impervious surfaces contributed most significantly to elevated temperatures, while vegetated and water-covered areas maintained cooling effects. UHI intensity was more pronounced in densely urbanized regions, highlighting the environmental strain caused by unregulated urban expansion. This research emphasizes the urgent need for sustainable urban planning and climate-resilient strategies to mitigate the UHI phenomenon in rapidly growing cities like Kandahar. The study further demonstrates the effectiveness of GIS and remote sensing for spatial analysis, offering actionable insights for urban planners and policymakers. These findings aim to guide efforts to balance urban growth with ecological preservation, ensuring sustainable development in the face of rising temperatures and climate challenges.

Keywords: Land surface; Temperature; Land use and land cover; GIS; Remote sensing; Urban Heat Island.

1. Introduction

Climate change is one of the most pressing global challenges of the 21st century, with its impacts increasingly evident worldwide [59]. Although the main cause of climate changes has been attributed to industrialized development of high-income countries. The rapid industrial growth of developing countries and its influence on raising the level of CO_2 emission should not be overlooked [2]. A

reduction in global CO_2 emissions was elected as one of the key SDGs to be achieved in this century by the UN. In addition to the urgent efforts to mitigate climate change, the cause of industrialization is further compounded by another serious pressing problem which is significant urbanization in developing countries. The urbanization that has taken place within developing nations has been done so quickly and, sometimes, unplanned compared with highly organized development within wealthy countries. This issue poses serious strains on local governments and places considerable pressure on natural resources. In turn leads to ecological, biophysical, and environmental changes due to the population increase [3]. Other adverse effects of urbanization are related to converting the land surface from permeable, such as agricultural lands, natural landscapes, and vegetation, to impermeable. For instance, cemented surfaces, leading the urban areas to become hotter than their surrounding rural or agricultural areas [4].

The UHI effect refers to the rise of temperature observed in urban areas relative to their rural surroundings due to the replacement of natural surfaces with artificial, impervious materials [5]. These materials, together with anthropogenic heat sources such as vehicles and infrastructure, increase heat storage and reduce evaporative cooling, leading to localized zones of intensified surface temperature. The UHI effect has been linked to ecological and climatic impacts, including the modification of microclimates and the amplification of broader warming trends [6]. Its magnitude is influenced by multiple factors, including urban form, population density, economic activity, and landscape configuration. As cities expand, these factors interact to increase surface temperatures, making UHI closely associated with metropolitan growth. Although urban expansion is not the sole determinant of UHI intensity, it accounts for a substantial proportion of observed variability in UHI patterns [7].

Economic development and population growth are the primary reasons for the expansion of urban areas, which are again linked to the final UHI outcomes. Land composition and landscape metrics influence the UHI effect, evidenced through many studies [8], [9], [10]. The LST defines the surface temperature of the land through radiation, which is defined by the amount of solar radiation. Urban Construction materials such as concrete, asphalt and metal, and infrastructural development has been accelerated [11]. The surface energy balance is significantly influenced by these construction materials as a result of their raised thermal conductivity [12]. In contrast, the replacement of vegetated landscape with urban setup leads to significant decline in the humidity level even though vegetation remains the prime contributor of moisture content in the atmosphere [13]. Rates of change that are high in the LULC should be observed to mitigate any adverse effects to human populations [14]. Quantification of such spatiotemporal changes in LULC needs to be done in the urban environment to quantify human activities interconnected with nature. This information on urban land use and its coverage change represents one of the first causes of monitoring human activities and development that can be used as a basis for creating future policies and directives concerning land uses. Moreover, it will enable responses to forecast changes in the magnitude of UHI. This approach reduce negative effects on urban environments due to LULC change [15].

Satellite image analysis offers high-resolution, consistent cover that is replicable; it can capture conditions of the Earth's surface. Urban climate analysis and decision-making facilitation are mainly based on remote sensing and geographic information systems [16]. A computer-assisted GIS was used in the present study to acquire and analyze multispectral and multitemporal satellite data. It enabled data gathering, maintenance, storage, and analysis, and presented organized data in a systematic map format. The impact of LULC change on land surface temperature was dealt with in the present study. Given the strong links between land use transformations, thermal behavior, and UHI dynamics, numerous empirical studies have investigated LULC, LST, and UHI relationships across different geographic settings. Reviewing these works provides valuable context for the present study and helps situate Kandahar within the broader field of urban climate research.

The influence of urban growth on LST in Kancheepuram was examined using a land surface temperature mapping approach [17]. Analysis of Landsat data from 1988 to 2021 showed that the

average LST increased by 152% over four decades. The authors reported that higher temperatures in the urban areas were primarily associated with the expansion of impervious surfaces and the reduction of vegetation. Further, researchers in Lahore, Pakistan [18], analyzed how urban development contributes to variations in UHI intensity. Changes in LULC classes from 1996 to 2016 were examined using remote sensing techniques, and the authors reported that built-up areas experienced approximately 6°C higher surface temperatures, with a temperature difference of about 4.8°C relative to nearby vegetated zones [18]. The authors reported that urban areas exhibited notably higher temperatures, with a mean UHI intensity of 5.5°C and peak values reaching 8.3°C. In another study, the UHI intensity in Baghdad was assessed using Landsat 8 imagery from July 2018 [19]. The authors reported temperature differences of up to 17°C between densely developed areas and zones dominated by vegetation or water. They concluded that the heightened UHI intensity was largely driven by vegetation loss, the use of low-albedo construction materials, urban design characteristics, and anthropogenic heat emissions [19]. Similarly, a study conducted in Guangzhou evaluated the use of GIS and remote sensing techniques for LST-based UHI analysis [20]. The authors stated that higher-elevation areas exhibited lower temperatures, while local climate zones E showed the highest surface temperatures [20]. These results provided valuable information for urban planners regarding the spatial severity of UHI within the city [20]. In addition, another study explored surface UHI patterns using GIS supported by both satellite and unmanned aerial vehicle (UAV) imagery [21]. The authors demonstrated that integrating multi-platform data improves the characterization of thermal hotspots, providing useful inputs for urban planning and for developing climate-resilient growth strategies [21].

Further evidence comes from Slovakia, where study [22] applied the MUKLIMO 3 model to evaluate UHI conditions in Bratislava and Trnava during a heatwave in August 2018. The authors found spatial variability, with temperature differences reaching up to 12°C in fragmented landscapes and 6°C in more uniform urban areas of Bratislava, while Trnava exhibited a maximum difference of 3°C. They reported that forests consistently displayed lower temperatures compared to the higher-temperature urban centers surrounding densely built-up zones. Similarly, a research study [23] assessed UHI risk in Greater Geelong, Australia [23]. Authors mapped thermal hotspots associated with low-vegetation areas, commercial zones, and high-density residential districts [23]. They found that UHI intensity was strongly correlated with population density, while building density had a weaker association [23]. The analysis provided useful insights for identifying urban areas most vulnerable to heat exposure [23]. In another study, [24] proposed a method for estimating LST and the UHI index in urban development land (UDL), China [24]. The LST showed an overall increasing trend over the past two decades, while UHI intensity initially declined and later rose as the city progressed through different stages of urban development (i.e. from clustered growth to a more uniform heat-island pattern) [24]. They also identified industry and logistics zones as major contributors to increased surface temperatures, highlighting their importance for UHI management in urban planning [24].

The reviewed literature consistently shows that urbanization, declining vegetation cover, and the multiplication of impervious surfaces contribute to rising LST and intensified UHI effects [25], [26]. However, despite global evidence, semi-arid regions such as Kandahar remained underexamined, especially in the context of post-conflict urban growth and limited environmental regulation. This study highlights the environmental concerns associated with fast-paced development in such settings. By focusing on Kandahar City, it offers insight into how urban expansion and LULC change contribute to localized warming and UHI intensification. The findings of this study will be useful for urban planners, policymakers, and environmental managers seeking to design heat-resilient development strategies. The demonstrated use of GIS and RS techniques signify their value for urban climate monitoring and decision-making, and their applicability across cities [27]. The primary objectives of this research are: (i) to analyze the spatiotemporal changes in LULC. (ii) to assess the

effects on LST in Kandahar City, Afghanistan, using remote sensing and GIS techniques. (iii) to map UHI intensity and identify thermal hotspots. The study contributes new insights into the thermal impacts of urbanization in semi-arid developing regions and provides actionable guidance for UHI mitigation and climate-responsive planning.

2. Materials and methods

Adopted methodology consisted of clear sequential flow that are presented as follows: initially electronic sources were explored, and a comprehensive literature review was conducted to identify the research gap and formulate the study objectives. Subsequently, the focus was concentrated on Kandahar City as the study area. Then, satellite imagery from the Landsat-5 Thematic Mapper (TM) and Landsat-8 Operational Land Imager (OLI) missions for the years 2008 and 2018 were obtained as the primary data source for LULC classification and LST estimation. The images were pre-processed using ArcGIS Pro software to apply geometric correction, radiometric calibration, and atmospheric correction, and to remove cloud cover and shadows [28]. Afterward, supervised classification was applied using the maximum likelihood algorithm, categorizing the land cover into four themes (built-up areas, vegetation, barren land, and water bodies). Training samples were selected based on field knowledge, Google Earth high-resolution imagery, and spectral characteristics. Subsequently, LST values were derived from the thermal bands of the Landsat images by converting digital numbers to top-of-atmosphere (TOA) radiance, then to brightness temperature, and finally applied surface emissivity corrections. At the end of processing phase, spatial analyses were performed to assess the relationship between LULC and LST changes by comparing the data from 2008 and 2018. Finally, hotspot analysis was conducted to identify areas with significant UHI intensities, while comparative analysis quantified the extent of urban expansion, vegetation loss, and associated temperature increases (Figure 1).

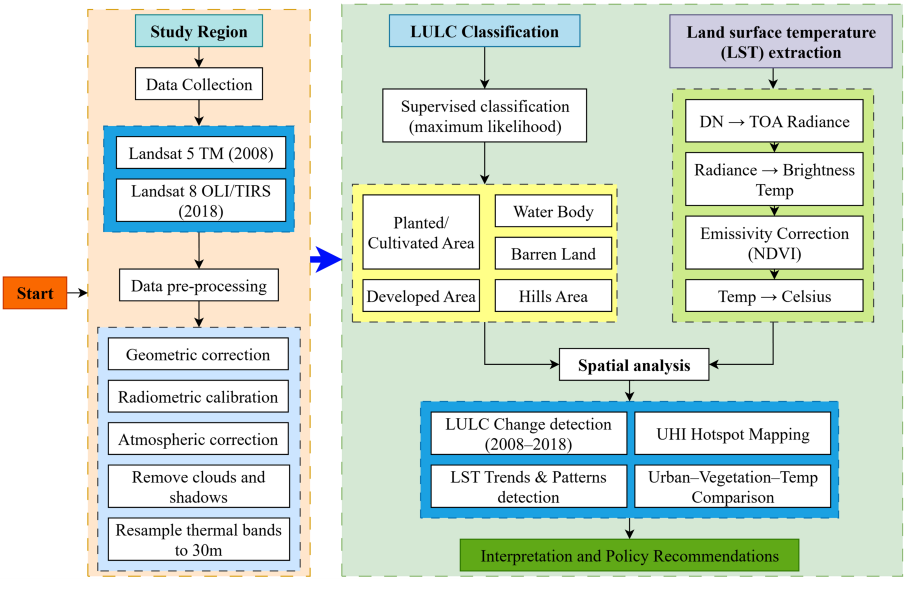

Figure 1: *Adopted methodology flowchart.*

2.1 Study Area

The study location, Kandahar City, is located within Kandahar province in southern Afghanistan, as shown in (Figure 2). The city lies approximately 500 kilometers southwest of Kabul (Capital of Afghanistan) and is located in the Arghandab river valley (this valley contributes to the regions' agricultural productivity). Kandahar province borders Zabul province to the northeast, Helmand province to the west, and Urozgan province to the north, and is located in close proximity to Pakistan, serving as a key transit corridor for trade and movement toward the southern border. The city is situated at an elevation of approximately 1010 meters above sea level, with predominantly flat terrain with minor hilly regions. Its geographical boundaries extend latitude of (31.45 to 31.75) and longitude of (65.58 to 65.82). The region experiences a semi-arid climate characterized by hot summers, mild winters with low precipitation [29], [30]. These climatic characteristics align with findings from other regions of Afghanistan, where persistent aridity, limited precipitation, and high rainfall variability have been widely reported [31], [32]. This region acts as the administrative, economic, and political zone of the country. Based on municipality the city is divided into 15 districts, each managing local services and administration. The city's land use includes agricultural areas, residential settlements, barren lands, and infrastructural settings. Study region is recognized as one of the principal commercial centers in southern Afghanistan, with its economy predominantly based on agriculture, trade, and small-scale industries.

2.2 Data Collection

In this research, both primary and secondary data sources were used. Where, the primary data includes satellite imagery of Kandahar city, which was obtained in cloud-free conditions from the United States Geological Survey (USGS) Landsat satellite archives [33]. Landsat images were obtained for two time periods, 2008 and 2018, covering a decade of urbanization and environmental changes in the region. For the year 2008, Landsat-5 Thematic Mapper (TM) data were used, comprising six reflective spectral bands suitable for LULC classification and one thermal band specifically designed for LST estimation. Bands 1–5 and 7, each with a spatial resolution of 30 meters, were used for LULC classification, while Band 6 (thermal band) with a spatial resolution of 120 meters was used for LST estimation. For the year 2018 the Landsat-8 Operational Land Imager and Thermal Infrared Sensor (OLI/TIRS), two thermal bands (Bands 10 and 11) with a thermal resolution of 100 meters were utilized for LST estimation, while bands 2–7 (30-meter resolution) and the panchromatic band (15-meter resolution) were used for LULC classification. The specifications of the satellite images and sensors employed are outlined in Table 1. Furthermore, secondary data were collected from various secondary sources, including published journal articles, thesis, books, reports, and contemporary research literature relevant to LULC changes and UHI phenomena, and remote sensing applications.

Table 1: *Satellite remote sensing data specifications used for LULC and LST mapping in 2008 and 2018.*

Year	Date Acquired	Path/rows	Satellite	Sensor ID	Required bands	Spatial resolution (m)	Thermal resolution
2008	23/5/2008	154/38	Landsat 5	TM	1, 2, 3, 4, 5 and 7	30	-
					6	-	120
2018	19/5/2018	154/38	Landsat 8	OLI	1, 2, 3, 4, 5, 6, 7, and 9	30	-
				TIRS	8	15	-
					10 and 11	-	100

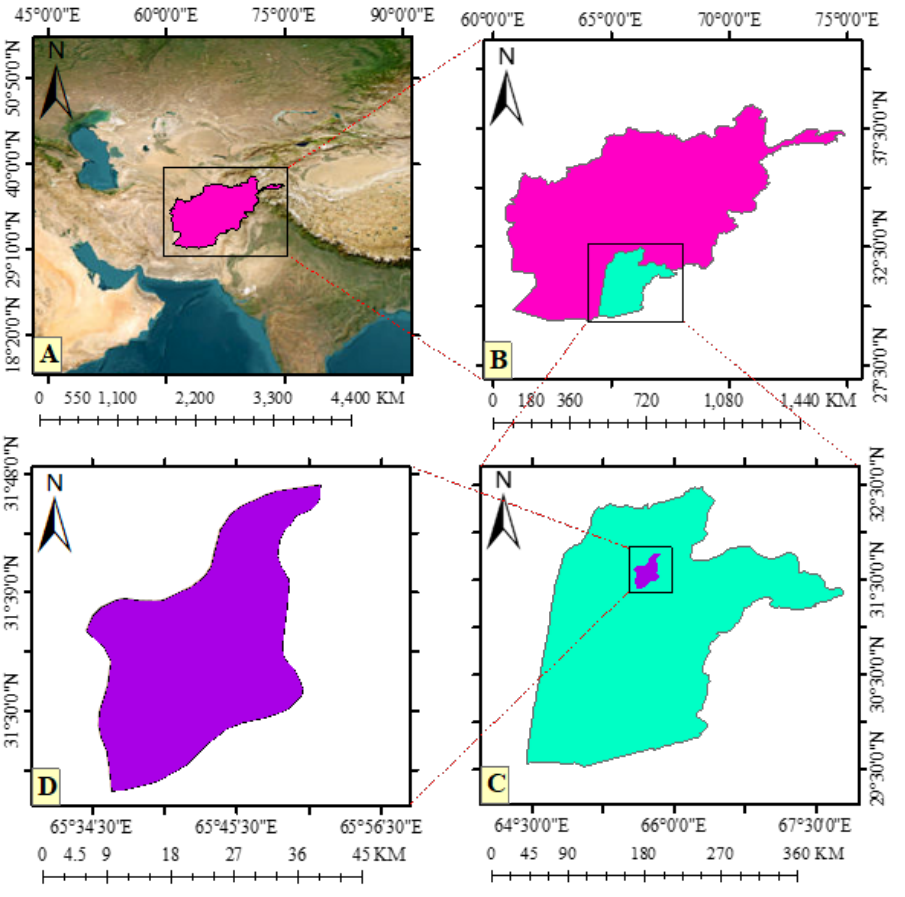

Figure 2: *Overview of the study area at multiple spatial scales; (A) Regional location of Afghanistan within Southwest Asia, with the national boundary highlighted, (B) National map of Afghanistan showing the Kandahar province outlined, (C) Enlarged view of the province with the city indicated, (D) Detailed map of the Kandahar city used for the case study.*

2.3 Data Examination

Data analysis followed a sequence of linked steps beginning with data pre-processing, which involved geometric correction, radiometric calibration, atmospheric adjustment of the satellite imagery, clouds and shadows removal, and resampling of thermal bands to 30 m for consistency between all obtained data from different sources (these steps clearly charted in the figure 1). After pre-processing, the multispectral bands were used in supervised classification to generate the LULC categories [34], while the thermal bands were processed in parallel to extract the LST values for each study year.

2.4 LST Extraction from Thermal Band

Landsat 8 OLI/TIRS contains two thermal bands (Bands 10 and 11) [35], while Landsat 5 TM includes one thermal band (Band 6) [36]. In this study, LST was extracted using Band 10 (as it is less affected by water vapor interference and produces more reliable LST values, according to USGS thermal calibration guidance) for Landsat 8 and Band 6 for Landsat 5. Band 11 of Landsat 8 was excluded following USGS recommendations due to its higher calibration uncertainty [37]. The Landsat 5 TM thermal band has a native spatial resolution of 120 m, which is resampled to 30 m

in Level-1 products, while Landsat 8 Band 10 was acquired at 100 m resolution. All thermal bands were resampled to 30 m to match the multispectral data used for LULC classification [38].

2.4.1 Landsat 8 OLI/TIRS Processing

The Level-1 Landsat data were used, which provide raw digital numbers (DN) and require radiometric preprocessing prior to land surface temperature derivation. Radiometric calibration was applied following USGS guidelines, and LST was derived directly from Level-1 thermal data without additional atmospheric correction (because Level 1 data already corrected by USGS itself, no need for any additional correction), ensuring consistency with standard USGS-recommended LST retrieval procedures [39]. It ensuring the measured radiance represents the surface energy rather than atmospheric interference. Following atmospheric correction, The raw Digital Numbers (DN) were converted to TOA spectral radiance using sensor-specific multiplicative (M_L) and additive (A_L) rescaling factors from the metadata [40], [41]:

$$L_\lambda = M_L \times Q_{cal} + A_L \tag{1}$$

where L_λ is the TOA spectral radiance $\left(\mathrm{W} \cdot \mathrm{m}^{-2} \cdot \mathrm{sr}^{-1} \cdot \mu\,\mathrm{m}^{-1}\right)$, Q_{cal} is the DN value, M_L is the radiance multiplicative scaling factor, and A_L is the radiance additive scaling factor [42].

The Brightness Temperature (BT) in Kelvin was then calculated from TOA radiance using the Planck equation and the thermal calibration constants K_1 and K_2 [43], [44]:

$$BT = \frac{K_2}{\ln\left(\frac{K_1}{L_\lambda} + 1\right)} \tag{2}$$

where $K_1 = 774.8853\ \mathrm{W} \cdot\ \mathrm{m}^{-2} \cdot \mathrm{sr}^{-1} \cdot \mu\,\mathrm{m}^{-1}$ and $K_2 = 1321.0789$ K for Landsat 8 [45]. Next, the Normalized Difference Vegetation Index (NDVI) was computed to estimate surface emissivity [46]:

$$NDVI = \frac{\text{Band}_5 - \text{Band}_4}{\text{Band}_5 + \text{Band}_4} \tag{3}$$

where Band 5 is the near-infrared (NIR) band and Band 4 is the red band.

The proportion of vegetation (P_v) was then determined as [47]:

$$P_v = \left(\frac{NDVI - NDVI_{\min}}{NDVI_{\max} - NDVI_{\min}}\right)^2 \tag{4}$$

where $NDVI_{\min}$ and $NDVI_{\max}$ are the minimum and maximum NDVI values in the image.

Surface emissivity (ε) was estimated using [48]:

$$\varepsilon = 0.004 \times P_v + 0.986 \tag{5}$$

Finally, the LST in degrees Celsius was obtained by applying emissivity correction to the brightness temperature [49], [50]:

$$LST\,(^\circ\mathrm{C}) = \frac{BT}{1 + (0.00115 \times BT/1.4388) \times \ln(\varepsilon)} - 273.15 \tag{6}$$

2.4.2 Landsat 5 TM Processing

For Landsat 5 TM , the single thermal band (Band 6) was used for LST estimation [51]. The TOA spectral radiance was calculated from digital number (DN) values using the sensorspecific rescaling parameters $L_{\min}$, $L_{\max}$, $QCAL_{\min}$, and $QCAL_{\max}$ provided in the metadata [52], [53]:

$$L_\lambda = \frac{(L_{\max} - L_{\min})}{(QCAL_{\max} - QCAL_{\min})} \times (QCAL - QCAL_{\min}) + L_{\min} \tag{7}$$

Brightness temperature (BT) in Kelvin was then derived from TOA radiance using the inverse Planck function [43], [44]:

$$BT = \frac{K_2}{\ln\left(\frac{K_1}{L_\lambda} + 1\right)} \tag{8}$$

where $K_1 = 607.76\ \mathrm{W} \cdot\ \mathrm{m}^{-2} \cdot \mathrm{sr}^{-1} \cdot \mu\,\mathrm{m}^{-1}$ and $K_2 = 1260.56$ K are the thermal calibration constants for Landsat 5 TM [52].

Surface emissivity (ε) was estimated using the same NDVI-based approach applied for Landsat 8, ensuring methodological consistency between sensors. The proportion of vegetation was first calculated from NDVI values, and emissivity was then derived using the formulation proposed by Joy Saha et al [54]. Finally, emissivity-corrected LST in degrees Celsius was calculated as [54]:

$$\mathrm{LST}\,(^\circ\mathrm{C}) = \frac{BT}{1 + \left(\frac{0.00115 \times BT}{1.4388}\right)\ln(\varepsilon)} - 273.15 \tag{9}$$

The calibrated LST maps for 2008 and 2018 were generated at 30 m spatial resolution, allowing direct comparison between the two periods. From these maps, minimum, maximum, and mean LST values, temperature ranges, and the spatial extent of high-temperature zones were extracted to support the analysis of spatial heating patterns and urban heat island dynamics in Kandahar city.

2.4.3 UHI Intensity

The UHI intensity was quantified by expressing each pixel's LST relative to the overall thermal characteristics of the study area. This approach standardizes the temperature field and highlights' locations that are anomalously warm or cool compared to the regional background. UHI intensity was therefore computed using a normalization formulation [55]:

$$\mathrm{UHI} = \frac{(LST - LST_m)}{SD} \tag{10}$$

where LST is the land surface temperature (°C) at each pixel, LST_m is the mean LST (°C) of the entire study area, and SD is the standard deviation of the LST distribution (°C). Positive values indicate surfaces warmer than the regional mean, whereas negative values showing cooler locations.

2.5 LULC Classification

A supervised classification approach (Support Vector Machine-SVM which is a GIS built-in feature through the Train Support Vector Machine Classifier tool) algorithm was implemented to categorize LULC in the region for the years 2008 and 2018. The Landsat satellite images lacked attribute tables, making classification into defined thematic categories a prerequisite for subsequent spatial and statistical analyses [34]. All image processing and classification were conducted within a GIS environment (ArcGIS Pro). The SVM classifier was configured with a radial basis function (RBF) kernel, which is well suited for handling non-linear separability in multispectral data. The penalty

parameter C was set to 100 and the kernel parameter was automatically optimized by the software to balance the generalization of the model and the accuracy of the classification.

For model calibration, training samples were manually selected for each LULC category based on field knowledge, high-resolution Google Earth imagery, and the distinct spectral characteristics of the land cover types. An initial set of 100 samples per class was used to construct the classification model. From this pool, a refined subset of 80 high-quality samples per class applied to the final classification of both 2008 and 2018 imagery. This protocol was designed to ensure classification consistency and enhance thematic accuracy, in line with established recommendations that the number and quality of training samples have a direct influence on the precision of supervised classification outputs [34]. The classification scheme comprised five major land cover categories relevant to the study area:

1. Developed areas (including buildings, roads, pavements, and permanent concrete structures).
2. Plant/Cultivated areas (encompassing farm fields, green spaces, and vegetated zones).
3. Barren land (areas devoid of vegetation cover).
4. Water bodies (including canals, rivers, and reservoirs).
5. Mountains and hills (elevated terrain and rocky outcrops).

To minimize spectral confusion between Plant/Cultivated areas and Barren land in the arid environment of Kandahar, NDVI thresholds were used to assist class separation, supported by visual interpretation of seasonal imagery. Areas exhibiting persistent low NDVI values were classified as Barren land, while higher NDVI values corresponding to active vegetation were assigned to the Plant/Cultivated class.

The SVM classifier was selected due to its proven ability to maximize separation between spectral classes through the construction of an optimal hyperplane in feature space [34]. This method is particularly effective for heterogeneous urban–rural mosaics such as Kandahar, where mixed pixels and subtle spectral differences can reduce the performance of less sophisticated classifiers.

2.5.1 Accuracy Assessment of LULC

Maintaining the accuracy of LULC maps is essential, as any spatial analysis remains incomplete without a clear understanding of the reliability of the classifications produced [34]. Accuracy levels between 85% and 90% are widely regarded as acceptable standards for distinguishing among land cover categories [34]. In the current research, a detailed accuracy assessment was conducted for the LULC maps generated for the years 2008 and 2018. To evaluate classification performance, a stratified random sampling approach was applied to ensure that all land cover categories were represented proportionally. A total of 150 reference points were allocated to each map, with the distribution proportional to the area of each class. The overall accuracy for each classification year was calculated following widely used accuracy assessment procedures using [34]:

$$A_p(\%) = \frac{N_c}{N_T} \times 100 \tag{11}$$

where $A_p(\%)$ denotes the overall accuracy, N_c is the number of correctly classified reference points, and N_T is the total number of validation points used in the assessment.

The resulting accuracy indicated strong classification performance for both periods. The 2008 LULC map achieved an overall accuracy of 91.40%, reflecting a high level of agreement between the classified categories and the reference data. The 2018 map yielded an overall accuracy of 88.75%, which remains within the acceptable range for rigorous land cover analysis. The comparative results demonstrate a slight reduction in classification accuracy in 2018, likely attributable to increased landscape heterogeneity and expansion of built-up areas over time.

3. Modeling Results

3.1 Analyzing the Spatiotemporal Shifts in LULC

The expansion of urban areas is particularly clear in classified images that extend from 2008 to 2018. At the same time, the rapid expansion of the population [56] has resulted in a decrease in the amount of agricultural and vegetative land. The findings indicate a substantial decrease in agricultural and vegetative land in the city center as a consequence of the establishment of new settlements. Specifically, planted/cultivated land decreased from 243.7 km² (38.62%) in 2008 to 175.5 km² (27.84%) in 2018, representing a reduction of 68.2 km² (10.78 %). The classified satellite imagery identified five major LULC classes: developed areas, planted/cultivated land, barren land, hills, and water bodies (Table 2 and Figure 3).

Table 2: *Land use patterns in Kandahar city for 2008 and 2018.*

	Planted/Cultivated Area		Developed Area		Water Body		Barren Land		Hills Area		
Year	KM2	(%)	KM2	(%)	KM2	(%)	KM2	(%)	KM2	(%)	Total
2008	243.7	38.62	133.82	21.2	12.50	1.98	130.92	20.75	110	17.43	630.94
2018	175.5	27.84	188	29.8	8	1.27	159	25.22	100	15.86	630.5

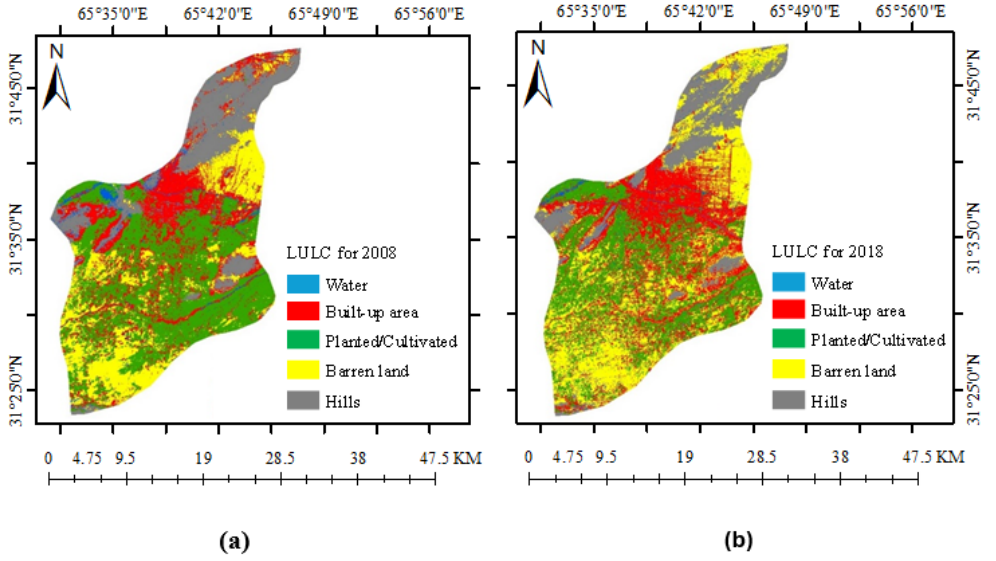

Figure 3: *LULC conditions in the study region for two observation years; (a) Spatial distribution of land cover classes for 2008, (b) Spatial distribution of the same land cover classes for 2018, illustrating the changes that occurred over the ten-year period.*

Clear spatial and temporal changes are evident between 2008 and 2018. Developed land increased from 21.20% $\left(133.82\ \text{km}^2\right)$ in 2008 to 29.80% $\left(188\ \text{km}^2\right)$ in 2018, reflecting urban expansion at high rate concentrated in the northern and central parts of the city. In contrast, planted and cultivated areas decreased from 38.62% $\left(243.7\ \text{km}^2\right)$ to 27.84% $\left(175.94\ \text{km}^2\right)$, showing significant loss of agricultural land. Barren land expanded from 20.75% ($130.92\ \text{km}^2$) to 25.22% $\left(159\ \text{km}^2\right)$, while water bodies declined from 1.98% to 1.27% of the total area. The shift from vegetated and agricultural surfaces toward impervious and sparsely vegetated land covers are obvious (Figure 4).

Overall, the results highlight a clear trajectory of urban growth and landscape transformation in Kandahar over the ten-year period.

3.2 LST Variability Change Detection Analysis

The statistical summary of estimated LST for 2008 showed that values range from 20.2450 °C to 38.2870 °C, with a mean of 30.1 °C. In comparison, LST values for 2018 range from 24.3936 °C to 41.7553 °C, indicated an overall shift toward higher surface temperatures over the ten-year period. Urban built-up areas, vacant land, and industrial zones consistently exhibit higher temperatures than agricultural land and water bodies between the years from 2008 to 2018 (Figure 5a and 5b). The maps also revealed a noticeable expansion of high-temperature zones in 2018, particularly in the central and northern parts of the city, where urbanization has intensified.

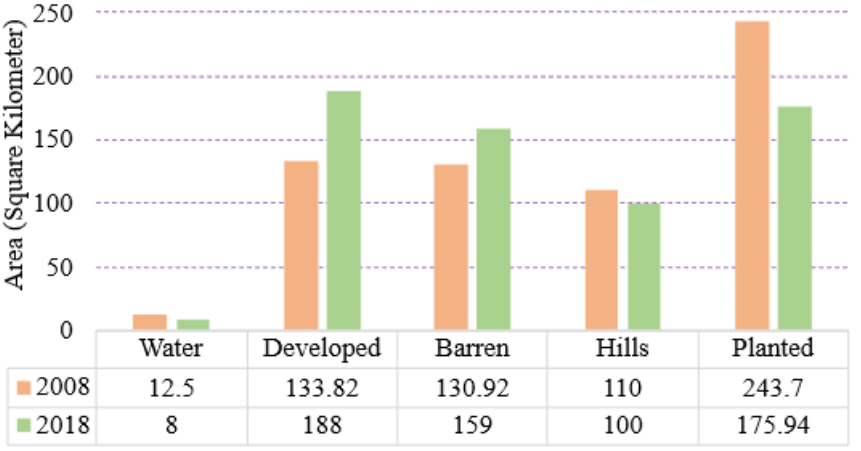

	Water	Developed	Barren	Hills	Planted
2008	12.5	133.82	130.92	110	243.7
2018	8	188	159	100	175.94

Figure 4: *Change detection for LULC classes in Kandahar city from 2008 to 2018.*

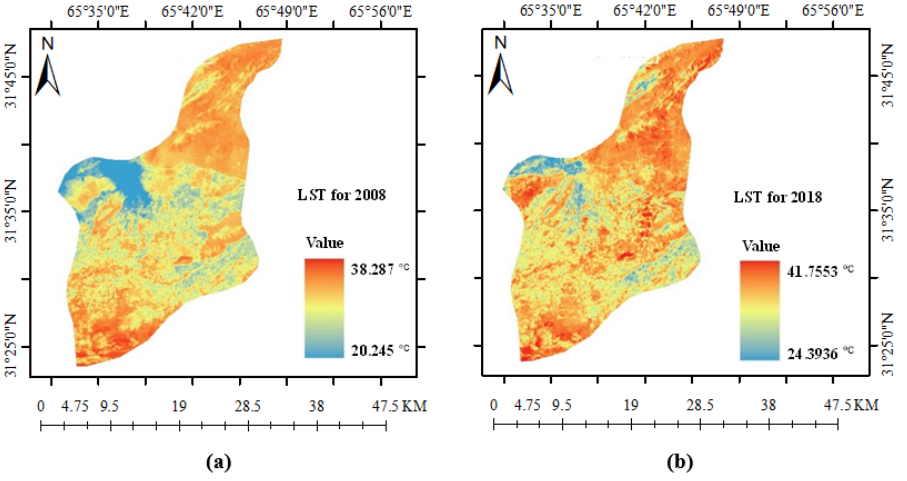

Figure 5: *Land surface temperature distribution in Kandahar city for two observed years; (a) spatial pattern of LST for the year 2008, (b) spatial pattern of LST for the year 2018.*

Temperature variations among land cover types are consistent with findings from previous studies supports that impervious surfaces retain more heat than vegetation or water due to differences in evapotranspiration, albedo, and surface moisture [57], [58]. While factors such as solar radiation and local meteorological conditions also influence LST patterns, the spatial comparison between 2008 to 2018 demonstrated that land use change the replacement of vegetated land with built-up surfaces plays a central role in shaping the observed temperature trends across the city.

Under the radiative transfer method which was used to determine the LST of the city, the results showed clear temperature differences among the LULC classes, with vegetated and agricultural areas exhibiting lower LST values and impervious surfaces such as buildings and paved areas showed higher temperatures. These patterns indicate that the replacement of vegetation with urban materials is associated with localized warming. Spatially, the most pronounced increase between 2008 to 2018 occurred in the expanding residential and commercial zones in the northern and central parts of the city, where vegetation loss was at its peak (Table 3).

Table 3: *LST changes detection for the year 2008 to 2018.*

Image Date	Lower Temperature (°C)	Higher Temperature (°C)	Mean Temperature (°C)
23/5/2008	20.245	38.287	30.1
19/5/2018	24.3936	41.7553	33.1

The LST were grouped into four classes covering the ranges (19–28) °C, (28–32) °C, (32–36) °C, and (36–41.75) °C, with each pixel assigned to a single class according to its boundary limits. The spatial pattern shows that the warmest class dominates large parts of the region, reflecting a shift toward higher temperature conditions that is consistent with long-term expansion of hotter surfaces driven by continued growth in built-up areas and the steady loss of vegetation, both of which reduce shading and evapotranspiration and allow heat to accumulate more easily during the day (Figure 6a). The area proportions confirm this shift: only 2.5 % of the land lies within the coolest range of (19–28) °C, and the intermediate temperature zones occupy 9.5 % and 41.3 % of the region, while the highest class of (36–41.75) °C accounts for 46.7 % of the total area. The large share of land in this upper range indicates that hotter surfaces have expanded at a faster rate than moderate or cooler zones, reflecting the combined influence of increasing urbanization, denser impervious surfaces, and declining plant cover. These changes have strengthened the temperature contrast across the landscape and intensified the heat load experienced at the surface, demonstrating a clear shift toward conditions that favor greater heat buildup and reduced natural cooling (Figure 6b).

3.3 Exploring the Impact of LULC on LST Patterns

A comparison of LULC patterns between 2008 and 2018 showed a notable expansion of developed areas and a reduction in planted and cultivated land. In 2008, vegetated surfaces covered a larger portion of the city, whereas many of these areas had been converted into built-up zones by 2018. This land conversion is consistent with the spatial shift observed in the LST observations. Where, agricultural and vegetated areas exhibited lower temperatures in 2008, while the same locations recorded higher temperatures in 2018 after they transformed into impervious surfaces. Similar relationships between impervious surface expansion and elevated LST have been widely documented in urban environments [57], [58]. Across both study years, surface temperatures varied systematically among LULC classes. Water bodies consistently demonstrated the lowest temperatures, followed by vegetated areas, while built-up and barren land displayed the highest temperature values. The temperature gradient observed in Kandahar aligns with the well-established thermal behavior of different land cover types, where moisture-rich, permeable surfaces remain cooler than hardened, impervious materials. These findings highlight the thermal consequences of land conversion and

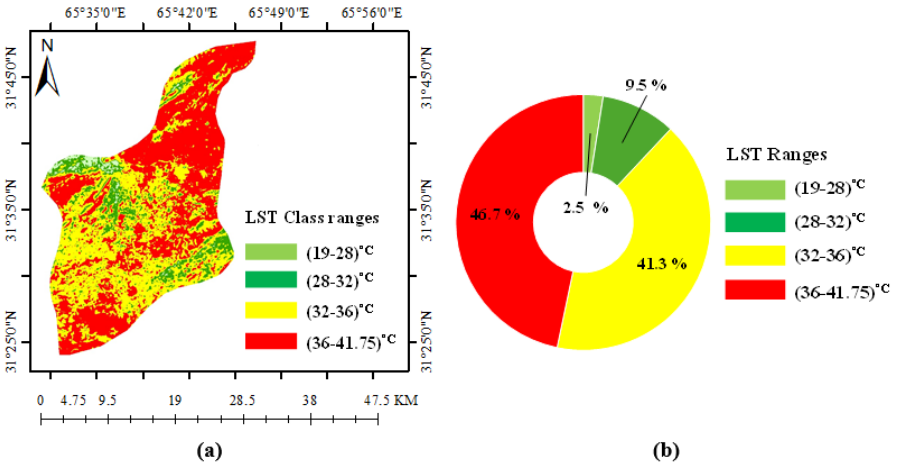

Figure 6: *Land surface temperature conditions in the study region during 2018; (a) Spatial distribution of LST classes across the region, (b) Percentage of Land Area Occupying Each Surface Temperature Class.*

underscore the importance of adopting sustainable land management strategies as urban development continues.

3.4 Assessing Settlement-Specific LST Dynamics

The expansion of settlements in Kandahar City between 2008 and 2018 led to clear changes in land surface temperatures. The mean LST increased from 30.1 °C in 2008 to 33.1 °C in 2018, with hotspot values reaching up to 41.75 °C in densely built-up zones. Areas that experienced high settlement expansion including new residential blocks, commercial corridors, and road networks consistently exhibited higher surface temperatures in 2018 compared to their 2008 values. This rise in temperature corresponds with changes in land cover patterns. Locations that were dominated by vegetation or agricultural land in 2008 showed lower LST ranges but recorded higher temperatures in 2018 after being converted to built-up or barren surfaces. Conversely, areas that retained vegetation or water cover remained among the coolest surfaces in both years. The spatial comparison therefore indicates a clear temperature gradient associated with land cover type. Therefore, these observations answer the question of how settlement expansion in Kandahar has contributed to localized surface warming. This warming likely originates from the replacement of cooler permeable surfaces with heat-retaining constructed materials.

3.5 Urban Heat Island Patterns Analysis

UHI intensity in 2018 followed a pronounced spatial pattern shaped by differences in land cover, with values ranging from 10.93 °C to 28.29 °C and the highest intensities occurring over densely built-up and sparsely vegetated surfaces where extensive impervious materials, reduced shading, and limited evaporative cooling promote greater heat storage during the day, while markedly lower intensities appeared over vegetation and water bodies where moisture availability and canopy cover moderate surface heating; this contrast is evident across the mapped domain, where compact urban areas and exposed soil consistently register the upper end of the intensity range and cooler surfaces cluster in greener zones, reflecting the combined influence of urban expansion, soil exposure, and vegetation decline on thermal buildup (Figure 7a). Transect-based profile (section A–A) further illustrates these relationships by showing repeated peaks where the line intersects built-up and bare

areas and drops where it passes through vegetated zones, thereby capturing the localized fluctuations in UHI magnitude along the 22,461 m section and demonstrating how surface characteristics govern heat accumulation at fine spatial scales (Figure 7b).

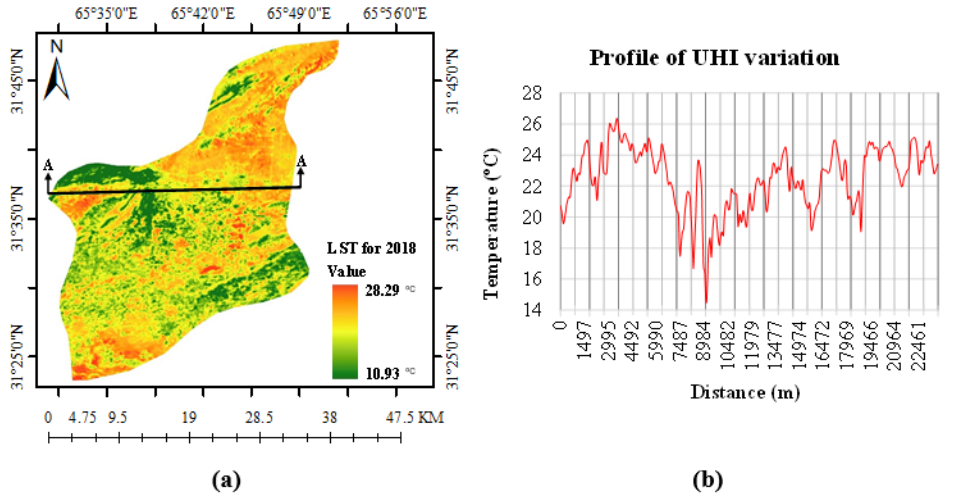

Figure 7: *UHI intensity patterns and their cross-sectional behavior across the study region for 2018; (a) Spatial distribution of UHI intensity expressed in degrees Celsius, with the A–A transect marking the section used to examine local variation, (b) UHI intensity profile along the A–A transect showing how the magnitude of the heat island shifts across the landscape.*

4. Discussion

The results of this study clearly demonstrate that Kandahar's urban expansion has produced distinct thermal consequences over the last decade. In the LULC analysis it observed that built-up areas increased from 21.20% to 29.80% between 2008 and 2018, while cultivated and vegetated land declined from 38.62% to 27.84%. These landscape transformations were accompanied by a rise in mean land LST of approximately 3 °C, with hotspot values exceeding 41.75 °C. Together, these outcomes reinforce the broader understanding that semi-arid cities are particularly sensitive to land cover modification because their natural cooling capacity is limited by sparse vegetation and high baseline temperatures. As a result, even very low reductions in green cover can trigger disproportionately large increases in surface heating.

This is consistent with findings from Ankara [59], where 57.57% decrease in green areas observed while 21.62% increase in urban areas detected, and 14.29% increase in UHI showed up, confirming that sustained impervious growth drives long-term surface warming [59]. Comparable trends were also reported in Sivas [60], where built-up area increased from 13.37% to 25.72% and UHI intensity rose from 6.77°C to 9.02°C, with water consistently provided the strongest cooling [60]. Similarly, Bengaluru [61] recorded urban growth from 4% to 43% between 1989 and 2017, with mean LST rising by ∼ 6°C, but partial cooling in core areas due to retained parks and water tanks [61], a contrast to Kandahar's uniformly high LSTs.

Evidence from Kandy [62] also supports the Kandahar's trend, as impervious cover increased from 2.3% to 23.9% between 1996 and 2017 and persistent surfaces (long-standing, densely developed zones) stayed 1.43°C warmer than newer ones, showing the lasting heat retention of older urban fabrics [62]. Furthermore, the thermal impact of industrial and extractive land uses seen in Kandahar is in parallel with Asansol-Durgapur [63], where settlement, industry, and coal mining expansion

between 1993 and 2015 raised summer LST in these zones by $\sim 6 - 7°C$ [63]. Additionally, correlations showed strong positive LST-NDBI and negative LST-NDVI relationships [63]. Dhaka [64], exhibited a similar negative LSTNDVI pattern, with built-up area increasing from 13.3% to 22.2% between 1990 and 2011 and mean LST increased from 20.7°C to 29.5°C [64], in alignment with the vegetation losswarming link observed in Kandahar. Moreover, in some regions partial contrasts are revealed due to water influence. In Okara [65], built-up area grew from 6.8% to 11.21% between 1991 and 2023 yet mean LST dropped to 8.97°C as water area expanded by 67.9%, demonstrating the cooling role of blue infrastructure [65]. In Pathumthani [66], mean LST fell from 37.4°C in 1997 to 31.3°C in 2018 during wetter years, then rose sharply to 38.5°C in 2023 under El Niño conditions, showing climate variability's ability to amplify or suppress UHI signals [66].

Consequently, across all cases, high-LST zones consistently aligned with built-up and barren surfaces, while vegetation and water moderated temperatures. Differences between regions were explained by variations in vegetation extent, water coverage, climatic anomalies, and urban form, but the overall evidence confirms that Kandahar's recent warming is primarily linked to high rate of impervious expansion and green cover loss.

5. Conclusion

The effects of LULC transformation on land surface temperature in Kandahar City between 2008 and 2018 were assessed. From the observed results, there is a clear transition toward more impervious surfaces. The built-up area expanded from 21.20% to 29.80%, while vegetative and agricultural lands declined from 38.62% to 27.84%. These changes were accompanied by a rise in mean LST from 30.1°C to 33.1°C, with hotspot temperatures reaching 41.75°C. Vegetated and water-covered areas kept the coolest surfaces, whereas dense urban zones firmly exhibited the highest thermal intensities. Together, these findings confirm that urbanization in a semi-arid environment significantly intensifies surface warming and strengthens the UHI effect.

The implications of these results highlight the growing vulnerability of Kandahar to heat stress and environmental degradations. As heat-absorbing surfaces expand and cooling areas disappear, the city loses much of its natural ability to regulate temperature. Because Kandahar already experiences high temperatures and has limited natural vegetation, it is essential to include heat-related considerations in future development and land use planning. Doing so will help improve urban resilience, protect public health, and support sustainable growth.

Based on these observations, we propose targeted recommendations to mitigate UHI intensity and guide future planning:

- Expand urban tree cover, parks, and vegetated corridors within identified hotspots to enhance shading and evapotranspiration.
- Encourage vertical greenery and rooftop gardens to compensate for reduced ground-level vegetation in dense districts.
- Incorporate small-scale blue infrastructure, such as retention ponds, into neighborhood planning.
- Promote the use of high-albedo and permeable materials for pavements, roofs, and building facades to reduce heat storage.
- Implement zoning regulations that limit unplanned expansion of impervious surfaces and protect remaining vegetated land.
- Integrate thermal performance criteria into building codes and development guidelines.
- Encourage urban agriculture initiatives where appropriate linking them directly to cooling and restoration of lost green space.

Collectively, these strategies are essential to strengthen urban resilience, reduce surface heat exposure, and support ecologically balanced development in Kandahar city as it continues to grow.

Abbreviations

LULC: Land Use Land Cover

LST: Land Surface Temperature
UHI: Urban Heat Island
GIS: Geographic Information System
RS: Remote Sensing
TM: Thematic Mapper (Landsat 5 sensor)
OLI: Operational Land Imager (Landsat 8 sensor)
TIRS: Thermal Infrared Sensor (Landsat 8 sensor)
DN: Digital Number
TOA: Top of Atmosphere
NDVI: Normalized Difference Vegetation Index
SVM: Support Vector Machine
K1, K2 : Calibration constants for radiance-to-temperature conversion
Lλ: Spectral radiance ($W/m^2/sr/\mu m$)
BT: Brightness Temperature (Kelvin)
ε: Surface emissivity
SD: Standard deviation (used in UHI index calculation)
USGS: United States Geological Survey

Availability of data and materials: Data used in this study are available from open access sources cited in the data collection section.

Acknowledgment: The authors acknowledge kind support from King Fahd University of Petroleum and Minerals.

Compliance with Ethical Standards

Competing Interests: The authors declare that they have no conflict of interest.

Reference

[1] P. Ogden, "Next Stop Glasgow: What the UN General Assembly Means for COP26," 2021.
[2] D. Khan and A. Ullah, "Testing the relationship between globalization and carbon dioxide emissions in Pakistan: does environmental Kuznets curve exist?," Environ. Sci. Pollut. Res., vol. 26, no. 15, pp. 15194–15208, 2019, doi: 10.1007/s11356-019-04913-9.
[3] U. Habitat, "Urbanization and Development: Emerging Futures," World Cities Rep., pp. 4–51, 2016.
[4] S. Gedik and S. Mugan-Ertugral, "The effects of marine tourism on water pollution," Fresenius Environ. Bull., vol. 28, no. 2, pp. 863–866, 2019.
[5] M. Borthakur and B. K. Nath, "A Study of Changing Urban Landscape and Heat Island Phenomenon in Guwahati Metropolitan Area," Int. J. Sci. Res. Publ., vol. 2, no. 11, pp. 169–174, 2012.
[6] D. Armson, P. Stringer, and A. R. Ennos, "The effect of tree shade and grass on surface and globe temperatures in an urban area," Urban For. Urban Green., vol. 11, no. 3, pp. 245–255, 2012, doi: 10.1016/j.ufug.2012.05.002.
[7] X. Li, Y. Zhou, G. R. Asrar, M. Imhoff, and X. Li, "The surface urban heat island response to urban expansion: A panel analysis for the conterminous United States," Sci. Total Environ., vol. 605–606, pp. 426–435, 2017, doi: 10.1016/j.scitotenv.2017.06.229.
[8] M. Nasar-u-Minallah, D. Haase, and S. Qureshi, "Evaluating the impact of landscape configuration, patterns and composition on land surface temperature: an urban heat island study in the Megacity Lahore, Pakistan," Environ. Monit. Assess., vol. 196, no. 7, p. 627, 2024.
[9] Z. Sun, Z. Li, and J. Zhong, "Analysis of the impact of landscape patterns on urban heat islands: A case study of Chengdu, China," Int. J. Environ. Res. Public Health, vol. 19, no. 20, p. 13297, 2022.

[10] L. Xiong, S. Li, B. Zou, F. Peng, X. Fang, and Y. Xue, "Long time-series urban heat island monitoring and driving factors analysis using remote sensing and geodetector," Front. Environ. Sci., vol. 9, p. 828230, 2022.
[11] J. John, G. Bindu, B. Srimuruganandam, A. Wadhwa, and P. Rajan, "Land use/land cover and land surface temperature analysis in Wayanad district, India, using satellite imagery," Ann. GIS, vol. 26, no. 4, pp. 343–360, 2020, doi: 10.1080/19475683.2020.1733662.
[12] H. M. Imran, J. Kala, A. W. M. Ng, and S. Muthukumaran, "Impacts of future urban expansion on urban heat island effects during heatwave events in the city of Melbourne in southeast Australia," Q. J. R. Meteorol. Soc., vol. 145, no. 723, pp. 2586–2602, 2019, doi: 10.1002/qj.3580.
[13] E. Igun and M. Williams, "Impact of urban land cover change on land surface temperature," Glob. J. Environ. Sci. Manag., vol. 4, no. 1, pp. 47–58, 2018, doi: 10.22034/gjesm.2018.04.01.005.
[14] A. D. I. Asmiwyati, R. Corner, "Seasonal comparison of Landsat ETM+ derived land surface temperature for southern Bali," p. 1152_1159, 2013.
[15] S. H. Rizvi, H. Fatima, M. J. Iqbal, and K. Alam, "The effect of urbanization on the intensification of SUHIs: Analysis by LULC on Karachi," J. Atmos. Solar-Terrestrial Phys., vol. 207, no. September 2019, p. 105374, 2020, doi: 10.1016/j.jastp.2020.105374.
[16] S. Pal and S. Ziaul, "Detection of land use and land cover change and land surface temperature in English Bazar urban centre," Egypt. J. Remote Sens. Sp. Sci., vol. 20, no. 1, pp. 125–145, 2017, doi: 10.1016/j.ejrs.2016.11.003.
[17] M. Bagyaraj et al., "A study of urban heat island effects using remote sensing and GIS techniques in Kancheepuram, Tamil Nadu, India," Urban Clim., vol. 51, no. April, p. 101597, 2023, doi: 10.1016/j.uclim.2023.101597.
[18] M. Imran and A. Mehmood, "Analysis and mapping of present and future drivers of local urban climate using remote sensing: a case of Lahore, Pakistan," Arab. J. Geosci., vol. 13, no. 6, p. 278, 2020.
[19] M. F. Abdulateef and H. A. S. Al-Alwan, "Assessment of surface urban heat island intensity and its causes in the city of Baghdad," IOP Conf. Ser. Mater. Sci. Eng., vol. 745, no. 1, 2020, doi: 10.1088/1757-899X/745/1/012162.
[20] X. Xu, W. Qiu, W. Li, D. Huang, X. Li, and S. Yang, "Comparing satellite image and GIS data classified local climate zones to assess urban heat island: A case study of Guangzhou," Front. Environ. Sci., vol. 10, no. November, pp. 1–18, 2022, doi: 10.3389/fenvs.2022.1029445.
[21] S. Dimitrov, A. Popov, and M. Iliev, "Mapping and assessment of urban heat island effects in the city of Sofia, Bulgaria through integrated application of remote sensing, unmanned aerial systems (UAS) and GIS," vol. 11524, p. 93, 2020, doi: 10.1117/12.2571967.
[22] J. Holec, J. Feranec, P. Šťastný, D. Szatmári, M. Kopecká, and M. Garaj, "Evolution and assessment of urban heat island between the years 1998 and 2016: case study of the cities Bratislava and Trnava in western Slovakia," Theor. Appl. Climatol., vol. 141, no. 3–4, pp. 979–997, 2020, doi: 10.1007/s00704-020-03197-1.
[23] P. Sidiqui et al., "Urban Heat Island vulnerability mapping using advanced GIS data and tools," J. Earth Syst. Sci., vol. 131, no. 4, 2022, doi: 10.1007/s12040-022-02005-w.
[24] X. Liang, X. Ji, N. Guo, and L. Meng, "Assessment of urban heat islands for land use based on urban planning: a case study in the main urban area of Xuzhou City, China," Environ. Earth Sci., vol. 80, no. 8, pp. 1–22, 2021, doi: 10.1007/s12665-021-09588-5.
[25] M. G. Gümüş and K. Gümüş, "Assessment of the impact of impervious surface increase on urban heat island and vegetation by remote sensing and statistical analysis: the case of Türkiye/Niğde city center (2013-2024)," Turkish J. Remote Sens., vol. 7, no. 1, pp. 69–90, 2025.
[26] Z. Zafar, Y. Zha, S. Fahd, and Y. Ji, "The interplay between urbanization, vegetation loss and surface heat island in cities: two decadal empirical evidence from Pakistan," Theor. Appl.

Climatol., vol. 155, no. 12, pp. 9911–9928, 2024.
[27] A. R. Bah, H. Norouzi, S. Prakash, R. Blake, R. Khanbilvardi, and C. Rosenzweig, "Spatial downscaling of GOES-R land surface temperature over urban regions: a case study for New York City," Atmosphere (Basel)., vol. 13, no. 2, p. 332, 2022.
[28] A. Sharma, S. R. Chopra, S. G. Sapate, and P. B. Bhagawati, "Algorithm For Preprocessing Satellite Imagery That Uses Geometric, Atmospheric, And Radiometric Correction," in 2025 International Conference on Emerging Smart Computing and Informatics (ESCI), IEEE, 2025, pp. 1–7.
[29] nomadseason, "Monthly climate in Kandahar, Afghanistan." Accessed: Dec. 11, 2025. [Online]. Available: https://nomadseason.com/climate/afghanistan/kandahar/kandahar.html
[30] Climate-Data, "Kandahar climate: Weather Kandahar temperature by month." Accessed: Dec. 11, 2025. [Online].
Available: https://en.climate-data.org/asia/afghanistan/kandahar/kandahar-1255/
[31] Z. H. Doost et al., "Development of intensity–duration–frequency curves for Herat, Afghanistan: enhancing flood risk management and implications for infrastructure and safety," Nat. Hazards, 2024, doi: 10.1007/s11069-024-06730-x.
[32] Z. H. Doost, A. Alsuwaiyan, A. Abdulraheem, N. M. Al-Areeq, and Z. M. Yaseen, "Rainfall Prediction Using Integrated Machine Learning Models with K-Means Clustering: A Representative Case Study of Harirud Murghab Basin-Afghanistan," IEEE Access, p. 1, 2025, doi: 10.1109/ACCESS.2025.3581921.
[33] USGS, "EarthExplorer." Accessed: Dec. 11, 2025. [Online].
Available: https://earthexplorer.usgs.gov/
[34] Z. H. Doost and Z. M. Yaseen, "The impact of land use and land cover on groundwater fluctuations using remote sensing and geographical information system: Representative case study in Afghanistan," Environ. Dev. Sustain., pp. 1–24, 2023, doi: 10.1007/s10668-023-04253-2.
[35] A. S. A. Nugraha, T. Gunawan, and M. Kamal, "Comparison of land surface temperature derived from Landsat 7 ETM+ and Landsat 8 OLI/TIRS for drought monitoring," in IOP Conference Series: Earth and Environmental Science, IOP Publishing, 2019, p. 12041.
[36] J. A. Barsi, S. J. Hook, J. R. Schott, N. G. Raqueno, and B. L. Markham, "Landsat-5 thematic mapper thermal band calibration update," IEEE Geosci. Remote Sens. Lett., vol. 4, no. 4, pp. 552–555, 2007.
[37] T. R. Loveland and J. R. Irons, "Landsat 8: The plans, the reality, and the legacy," Remote Sens. Environ., vol. 185, pp. 1–6, 2016.
[38] USGS, "What are the band designations for the Landsat satellites? | U.S. Geological Survey." Accessed: Dec. 11, 2025. [Online]. Available: https://www.usgs.gov/faqs/what-are-band-designations-landsat-satellites
[39] D. Antoine and A. Morel, "A multiple scattering algorithm for atmospheric correction of remotely sensed ocean colour (MERIS instrument): principle and implementation for atmospheres carrying various aerosols including absorbing ones," Int. J. Remote Sens., vol. 20, no. 9, pp. 1875–1916, 1999.
[40] R. Gens and J. C. Rosselló, "8 Remote Sensing Data," Remote Sens. Handbook, Vol. I Sensors, Data Norm. Harmon. Cloud Comput. Accuracies, p. 274, 2024.
[41] P. O. Ibrahim, A. A. Adesaanu, and E. E. Eyo, "Satellite derived bathymetry of Kainji Dam," School of Environmental Technology International Conference Proceedings, 2024, 2024.
[42] D. D. Ngoc et al., "Atmospheric correction algorithm over coastal and inland waters based on the red and NIR bands: application to Landsat-8/OLI and VNREDSat-1/NAOMI observations," Opt. Express, vol. 27, no. 22, pp. 31676–31697, 2019.
[43] M. Isaya Ndossi and U. Avdan, "Application of open source coding technologies in the production of land surface temperature (LST) maps from Landsat: a PyQGIS plugin," Remote

Sens., vol. 8, no. 5, p. 413, 2016.
[45] B. K. Veettil, V. Puri, D. D. Van, and N. X. Quang, "Variations in land surface temperatures in small-scale urban areas in Vietnam during Covid-19 restrictions: Case studies from Da Nang, Hue and Vinh City," Environ. Monit. Assess., vol. 195, no. 7, p. 822, 2023.
[46] S. Huang, L. Tang, J. P. Hupy, Y. Wang, and G. Shao, "A commentary review on the use of normalized difference vegetation index (NDVI) in the era of popular remote sensing," J. For. Res., vol. 32, no. 1, pp. 1–6, 2021.
[47] D. Maroni et al., "Land surface temperature and vegetation index as a proxy to microclimate," J. Environ. Chem. Eng., vol. 9, no. 4, p. 105796, 2021.
[48] K. K. Singh, M. Parida, and G. Jasrotia, "Urbanization induced land use/land cover change and its impact on land surface temperature in Bhubaneshwar city, India," Acta Geogr. Debrecina Landsc. Environ. Ser., vol. 18, no. 2, pp. 43–62, 2024.
[49] B. P. Kumar, K. R. Babu, B. N. Anusha, and M. Rajasekhar, "Geo-environmental monitoring and assessment of land degradation and desertification in the semi-arid regions using Landsat 8 OLI/TIRS, LST, and NDVI approach," Environ. Challenges, vol. 8, p. 100578, 2022.
[50] W. Al-Shaar, O. Bonin, G. Faour, N. Zeidan, and M. Al-Shaar, "Spatial analysis of land surface temperature distribution: case of the Greater Beirut Area," Euro-Mediterranean J. Environ. Integr., vol. 7, no. 4, pp. 483–495, 2022.
[51] G. Chander and B. Markham, "Revised Landsat-5 TM radiometric calibration procedures and postcalibration dynamic ranges," IEEE Trans. Geosci. Remote Sens., vol. 41, no. 11, pp. 2674–2677, 2003.
[52] S. Guha, H. Govil, and S. Mukherjee, "Long-term evaluation of land surface temperature with bare surface index and surface vegetation index: a case study of a central Indian city," Pap. Appl. Geogr., vol. 9, no. 4, pp. 425–441, 2023.
[53] F. Yuan and M. E. Bauer, "Comparison of impervious surface area and normalized difference vegetation index as indicators of surface urban heat island effects in Landsat imagery," Remote Sens. Environ., vol. 106, no. 3, pp. 375–386, 2007.
[54] J. Saha, S. S. Ria, J. Sultana, U. A. Shima, M. M. H. Seyam, and M. M. Rahman, "Assessing seasonal dynamics of land surface temperature (LST) and land use land cover (LULC) in Bhairab, Kishoreganj, Bangladesh: A geospatial analysis from 2008 to 2023," Case Stud. Chem. Environ. Eng., vol. 9, p. 100560, 2024.
[55] A. Malik and G. Kalotra, "Land surface temperature and Urban heat Island: A case study of Faridabad City using RS and GIS techniques," vol, vol. 6, pp. 1–12, 2024.
[56] World Population Review, "Kandahar Population 2025." Accessed: Dec. 06, 2025. [Online]. Available: https://worldpopulationreview.com/cities/afghanistan/kandahar?utm_*source* = *chatgpt.com*
[57] S. Vujovic, B. Haddad, H. Karaky, N. Sebaibi, and M. Boutouil, "Urban heat island: Causes, consequences, and mitigation measures with emphasis on reflective and permeable pavements," CivilEng, vol. 2, no. 2, pp. 459–484, 2021.
[58] X. Li, Y. Li, S. Di, Y. Niu, and C. Zhang, "Evapotranspiration and land surface temperature of typical urban green spaces in a semi-humid region: Implications for green management," Front. Environ. Sci., vol. 10, p. 977084, 2022.
[59] R. Bovkir, "GIS-BASED APPROACH TO ASSESSING LAND USE CHANGE IMPACTS ON URBAN HEAT ISLAND PATTERNS," As İzmir Kâtip Çelebi Univ. Artif. In-telligence Data Sci. Appl. Re.
[60] C. B. Karakuş, "The impact of land use/land cover (LULC) changes on land surface temperature in Sivas City Center and its surroundings and assessment of Urban Heat Island," Asia-Pacific J. Atmos. Sci., vol. 55, no. 4, pp. 669–684, 2019.
[61] N. R. Govind and H. Ramesh, "The impact of spatiotemporal patterns of land use land

cover and land surface temperature on an urban cool island: a case study of Bengaluru," Environ. Monit. Assess., vol. 191, no. 5, p. 283, 2019.
[62] D. Dissanayake, T. Morimoto, M. Ranagalage, and Y. Murayama, "Land-use/land-cover changes and their impact on surface urban heat islands: Case study of Kandy City, Sri Lanka," Climate, vol. 7, no. 8, p. 99, 2019.
[63] D. Choudhury, K. Das, and A. Das, "Assessment of land use land cover changes and its impact on variations of land surface temperature in Asansol-Durgapur Development Region," Egypt. J. Remote Sens. Sp. Sci., vol. 22, no. 2, pp. 203–218, 2019.
[64] A. M. Dewan and R. J. Corner, "Impact of land use and land cover changes on urban land surface temperature," in Dhaka megacity: Geospatial perspectives on urbanisation, environment and health, Springer, 2013, pp. 219–238.
[65] X. Duan et al., "A geospatial and statistical analysis of land surface temperature in response to land use land cover changes and urban heat island dynamics," Sci. Rep., vol. 15, no. 1, p. 4943, 2025.
[66] P. Thammaboribal, "Investigating Land Surface Temperature Variation and Land Use Land Cover Changes in Pathumthani, Thailand (1997-2023) using Landsat Satellite Imagery: A Comprehensive Analysis of LST and Urban Hot Spots (UHS)," Int. J. Geoinformatics, vol. 20, no. 2, pp. 27–41, 2024.